

# Chandra and XMM-Newton observations of the exceptional pulsar PSR B0628-28

E. Tepedelenlioğlu<sup>1</sup>

`emre@cow.physics.wisc.edu`

and

H. Ögelman<sup>1,2</sup>

`ogelman@cow.physics.wisc.edu`

## ABSTRACT

PSR B0628-28 is a radio pulsar which was first detected in the X-ray band by *ROSAT* and then later observed with *Chandra* and XMM-Newton. The *Chandra* observation yielded an X-ray luminosity two orders of magnitude higher than what is expected for spin-powered pulsars, also there were no pulsations detected. The XMM-Newton observation, however, reveals pulsations at the expected radio period,  $P = 1.244$  s. The simultaneously analyzed spectra also gives a luminosity (in cgs)  $\log L_X = 30.34$ , which is  $\sim 350$  times greater than what would be expected from the correlation between  $L_X$ - $\dot{E}$ . We present the timing and spectral analysis of the combined *Chandra* and XMM-Newton archival data.

## 1. Introduction

PSR B0628-28 is an old pulsar that has a characteristic age ( $\tau = P/2\dot{P}$ ) of 2.8 Myr. Since older pulsars have radiated away their initial heat content and have relatively low rotational energy loss ( $\dot{E} = I\Omega\dot{\Omega}$ ), one would expect to detect X-ray radiation coming from the reheating of the surface (e.g. see Tsuruta 1998; Shibasaki & Lamb 1989). In young pulsars, however, thermal radiation from the neutron star surface is dominated by the nonthermal component from the neutron star magnetosphere, whose spectrum can be described primarily by a power-law model. We, also, know from X-ray observations that the pulsar's nonthermal luminosity ( $L_X$ ) shows a correlation with the spin-down power  $\dot{E}$ . For instance, Possenti *et al.* (2002) found a best fit based on 37 pulsars. Although the variance is large, pulsars follow a general trend that can be formulated as  $\log L_X^{2-10} = 1.34 \log \dot{E} - 15.34$ . This set included only three old ( $\tau > 10^6$  years) pulsars. The reason for having only three is two fold. The first one is that older pulsars are less active and relatively cooler, hence most of them were not detected until *Chandra* and XMM-Newton. The

---

<sup>1</sup>Department of Physics, University of Wisconsin-Madison, 1150 University Ave., Madison, WI 53703, USA

<sup>2</sup>Faculty of Engineering and Natural Sciences, Sabancı University, Orhanlı Tuzla, İstanbul 34956, Turkey

detected ones have low countrates, consequently statistically poor spectra. This makes it challenging to distinguish between spectral models. The other reason is that it is expected that surface emission from old neutron stars will be dominant, resulting in spectra to be more like a blackbody. Hence, the X-ray radiation from these pulsars are not expected to be characterized by a power-law model. However, recent observation of PSR B0943+10 (Zhang *et al.* 2005), PSR B0823+26, PSR B0950+08, PSR J2043+2740 with XMM-Newton (Becker *et al.* 2004) and of PSR B2224+65 with *Chandra* (Zavlin & Pavlov 2004) has unfolded a new perspective in understanding old neutron stars. Not only many previously undetected sources were detected but also it has been possible to distinguish between different spectral models. These old pulsars have spectra that is best described by a power-law model, as opposed to a black-body model. Young pulsars that are powered by their spin-down all have power-law indices  $\Gamma$  between the narrow range 1.4-2.3. On the other hand, recent observations of old pulsars have shown that they have steeper spectra. The power-law indices derived from spectral fits are in the range  $\Gamma \sim 1.7\text{--}3.1$ . This phenomenon is interesting in that it suggests the possibility that  $\Gamma$  can be a function of the age of the pulsar. As the age increases the spectrum becomes steeper.

PSR B0628-28 is the longest period radio pulsar detected in X-rays. However, physical parameters inferred from radio observations are not in any means extreme. The *Chandra* data yielded a luminosity two orders of magnitude greater than what is expected for a spin-powered pulsar (Ögelman & Tepedelenlioğlu 2004). The varying efficiency of converting spin-power in to X-ray luminosity in pulsars can be explained by geometrical effects. But, none of these can amount to such a great excess flux in the X-ray band. In this paper we try to address the reasons for this extreme luminosity. We describe the XMM-Newton and *Chandra* data in § 2 and present the result of our timing and spectral analysis in § 3. We discuss the implications of the analysis results in § 4.

## 2. *Chandra* and XMM-Newton observations of PSR B0628-28

### 2.1. *Chandra*

PSR B0628-28 was observed twice, first on 2001 November 04 and again on 2002 March 25 for 2000 s and 17000 s, respectively. For both observations photons were collected using the Advanced CCD Imaging Spectrometer (ACIS). Data were collected in the nominal timing mode, with 1.141 s exposures between CCD readouts. We reprocessed the Level 1 event data to correct the detrimental effects of charge transfer efficiency. The imaging, timing and spectral analysis presented here were done only on the 17 ks observation, the 2.0 ks observation was disregarded due to an interruption by a large solar storm. The background countrate during this solar storm increased by a factor of  $\sim 20$ . The net source countrate during the first observation period was  $0.011 \pm 0.001$  counts per second (cps) where the error is in the 68% confidence range. Since by taking into account the 2.0 ks observation we gain only  $\sim 27$  counts, which is not enough to improve our statistics significantly, we preferred to disregard these counts, which potentially can be misleading.

The measured PSF of PSR B0628-28 is consistent with the ACIS point-source response, hence the ACIS image reveals a point-like X-ray source at the pulsar position. The Chandra position of PSR B0628-28 is  $\alpha = 06^{\text{h}}30^{\text{m}}49\overset{.}{4}3$ ,  $\delta = -28^{\circ}34'43\overset{.}{6}0$  (J2000.0), which considering  $0\overset{.}{5}$  rms error and the  $\sim 0\overset{.}{6}$  absolute astrometric accuracy of *Chandra*, is in good agreement with the radio position  $\alpha=06^{\text{h}}30^{\text{m}}49\overset{.}{5}3$ ,  $\delta = -28^{\circ}34'43\overset{.}{6}0$  (J2000.0), which was taken from the ATNF pulsar catalogue<sup>1</sup>.

## 2.2. XMM-Newton

PSR B0628-28 was observed with XMM-Newton on 2004 February 28 for a total ontime of 48 ks. MOS1/2 were both operated in imaging (PrimeFullWindow) mode and the medium filter was used. During the EPIC-pn exposure the thin filter was used and the detector was operated in imaging (PrimeLargeWindow) mode for 47 ks. The temporal resolution achieved with this choice of science modes were 2.6 s and 43 ms for MOS1/2 and pn, respectively.

The background of EPIC camera is known to be effected by soft proton flares. In order to screen for times of high background we inspected the light curves of MOS1/2 and pn data separately at energies above 10 keV. Both sets of data were effected by high background. The light curves were formed with 100 s bins and after inspection we rejected bins with countrate greater than 0.4 cps. The removal of high background time intervals from the data leaves us with effective exposure times of 42.5 ks and 33.3 ks for MOS1/2 and pn, respectively. The pulsar is clearly detected in the EPIC image at  $\alpha = 06^{\text{h}}30^{\text{m}}49\overset{.}{4}8$ ,  $\delta = -28^{\circ}34'43\overset{.}{1}0$  (J2000.0) which differs from the radio position by only  $0\overset{.}{8}$  well within the  $2\overset{''}-3\overset{''}$  uncertainty of the EPIC absolute astrometry. The shape of the radial profile of the source is also consistent with that expected for a point-like source.

## 3. Results

### 3.1. Timing

For searching pulsations from PSR B0628-28 *Chandra* ACIS and XMM-Newton EPIC-MOS data were not suitable due to their limited temporal resolution. The sampling frequency in both cases set by the detector read out rate give a Nyquist frequency greater than the pulsar frequency (see Table 1). Thus we used EPIC-pn data that has 43 ms timing resolution.

We extracted source plus background photons from a  $30''$  radius circle centered at the pulsar position, which encircles about 85% of all detected source counts. The extraction region contained 1047 counts of which 16% is background. The photon arrival times were solar system barycenter corrected. The pulsar's spin parameters (Table 1) are well known from radio observations and can

---

<sup>1</sup><http://www.atnf.csiro.au/research/pulsar/psrcat>

be extrapolated to the mean epoch of the XMM-Newton observation: MJD=53063.339. Around this predicted pulsar frequency, we then generated a periodogram using the  $Z_1^2$ -statistic. The X-ray periodogram is shown in Figure 1. We found a peak at  $f = 0.80358444 \pm 0.00000112$  Hz which is consistent with the extrapolated pulsar frequency  $f = 0.80358551$  Hz. The  $Z_1^2$  for this peak is 40.4, which has a probability of chance occurrence of  $1.69 \times 10^{-8}$ . The pulse profile of PSR B0628-28 over the whole energy band (bottom panel in Figure 2) is broad and single-peaked with a pulse fraction of  $f_p = 35 \pm 12\%$ . Here we defined the pulse fraction as  $(C_{\max} - C_{\min})/(C_{\max} + C_{\min})$ , where  $C_{\max}$  and  $C_{\min}$  are the maximum and minimum counts per bin, respectively.

We also looked at the pulse profile of the pulsar at different energy bands (upper panels of Figure 2). Most of the counts are in the soft band, 67% and 87% of all counts are in the 0.2-1 and 0.2-2 keV energy bands, respectively. Pulsed fraction in each selected energy band seems to be consistent with each other within the  $1\sigma$  errors associated. The pulse shape does not seem to be energy dependent which would suggest that all pulsed X-rays are coming from the same region.

### 3.2. Spectral

The pulsar's energy spectrum was extracted from the MOS1/2 data by selecting all events detected in a circle of radius  $50''$  centered on the pulsar position. This region includes 90% of all event from the pulsar. Due to a source located close to the pulsar we extracted the background spectrum from a nearby circular region with radius  $87''$ . For the EPIC-pn data we extracted the spectrum from a circle centered on the pulsar with radius  $30''$  (includes 80% of source counts). PSR B0628-28 was being located very close to the chip boundary precluded the extraction of the background spectrum from an annular region around the pulsar. Hence, we used an off-source circular region with radius  $66''$ .

To extract the spectrum from the *Chandra* data we used a circular region centered on the pulsar position with  $2''$  radius. This region contains 95% of all source counts. The background spectrum was extracted from an annulus of radii  $3'' < r < 50''$ .

In total, the extracted spectra include 780 EPIC-pn source counts and 754 EPIC-MOS1/2 source counts. Both spectra were binned so that each bin contained minimum 25 counts per bin. *Chandra* data had a total of 184 source counts. The extracted photons were binned and regrouped such that each fitted spectral bin contained minimum of 20 counts. All three extracted spectra were then simultaneously fitted with model spectra.

Among the single-component spectral models, an absorbed power-law model gave the statistically best representation ( $\chi^2 = 56.2$  for 62 degrees of freedom (dof)) of the observed spectrum. A single black-body ( $\chi^2 = 93$  for 62 dof) did not give a statistically acceptable fit. This fit when absorbing column is left to vary also yields a very low  $N_{\text{H}}$ . The best fit power-law spectrum and residuals are shown in Figure 3.

The power-law model yields a column density of  $N_{\text{H}} = 1.38_{-0.23}^{+0.37} \times 10^{21} \text{ cm}^{-2}$ , a photon index  $\Gamma = 3.20_{-0.23}^{+0.26}$ , and a normalization of  $1.73_{-0.22}^{+0.26} \times 10^{-5} \text{ photons cm}^{-2} \text{ s}^{-1} \text{ keV}^{-1}$  at  $E = 1 \text{ keV}$ . The errors are the upper and lower bounds of the  $1\sigma$  confidence range. The normalization converts to an unabsorbed energy flux of  $f_{\text{X}}^{2-10} = 8.61_{-0.33}^{+2.15} \times 10^{-15} \text{ erg cm}^{-2} \text{ s}^{-1}$  in the 2-10 keV band. Given the distance of  $d = 1.45 \text{ kpc}$  this yields an X-ray luminosity of  $L_{\text{X}}^{2-10} = 2.17_{-0.07}^{+0.56} \times 10^{30} \text{ erg s}^{-1}$ . This luminosity implies a rotational energy to X-ray energy conversion factor  $L_{\text{X}}/\dot{E} = 0.015$  within 2-10 keV band.

It is natural to assume that, in addition to the magnetospheric emission, thermal emission from polar caps or from the surface due to reheating of the superfluid interior contributes to the observed X-ray flux. In order to explore this possibility and how it represents the data we used a two component model, thermal and magnetospheric, to fit the spectra. As a first approach we let every parameter vary. The fit gives a blackbody temperature of  $T = 3.28_{-0.62}^{+1.31} \times 10^6 \text{ K}$  and effective radius  $R = 59_{-46}^{+65} \text{ m}$ . The power-law photon index does not change significantly and has a value of  $\Gamma = 2.98_{-0.65}^{+0.91}$ . The bolometric luminosity of the thermal component is  $L_{\text{bol}} = 2.87 \times 10^{30} \text{ erg s}^{-1}$  whereas the total luminosity in the 2-10 keV is  $L_{\text{X}}^{2-10} = 1.67_{-0.62}^{+0.91} \times 10^{30} \text{ erg s}^{-1}$ . The nonthermal X-ray luminosity in the 2-10 keV band converts to an X-ray efficiency of  $L_{\text{X}}/\dot{E} = 0.01$ . The hydrogen column density is not well bound  $N_{\text{H}} = 0.62_{-0.62}^{+0.98} \times 10^{21} \text{ cm}^{-2}$  but still is consistent with the estimate obtained from the single power-law fit. The quality of the composite model ( $\chi^2 = 54.5$  for 62 dof) is slightly better than that obtained from single power-law model. However, both fits are statistically acceptable and addition of a new model will always tend to decrease the  $\chi^2$ .

#### 4. Discussion

With the observations of new sensitive X-ray telescopes like XMM-Newton and *Chandra* we are uncovering a class of new sources; X-ray luminous old-radio pulsars. Up to now there are only seven such sources that have been detected. Namely, these are PSRs B2224+65, J2043+2740, B1929+10, B0823+26, B0950+08, B0943+10 and B0628-28 (see Zavlin & Pavlov 2004; Becker *et al.* 2004; Zhang *et al.* 2005; Ögelman & Tepedelenlioğlu 2004). Of these six sources only three of them (PSRs B0950+08, B0823+26, B0628-28) have high quality spectra so that one can distinguish between spectral models (e.g. thermal vs. nonthermal). Becker *et al.* (2004) suggested that the three pulsar observed with XMM-Newton (PSRs B0950+08, 0823+26, J2043+2740) all have spectra described better by a single power-law model, indicating nonthermal emission is dominant. Zavlin & Pavlov (2004) arrived at the same conclusion for the pulsar PSR B2224+65 from the analysis of the *Chandra* ACIS observation. All these pulsars have X-ray luminosities greater than what is predicted from the correlation between  $L_{\text{X}}^{2-10} \cdot \dot{E}$  (Possenti *et al.* 2002). For example, in the case of PSR B0628-28 and PSR B2224+65 the luminosities inferred from spectral fits are greater than the so-called “maximum efficiency line” derived by Possenti *et al.* (2002) such that all pulsar lie below this line in the  $\log L_{\text{X}} \text{-} \log \dot{E}$  plane. PSR B0628-28 has been known to be an exceptional emitter

and with the detection of pulsations from this source at the radio frequency has left no doubt that it is the X-ray counterpart of the pulsar. These luminous old pulsars (in particular PSR B0628-28) seem not to follow the trend their possible progenitors do. Which suggests that pulsars become more X-ray efficient as they grow older, given that  $\tau$  is inversely proportional to  $\dot{E}$ .

As mentioned in § 1, Possenti *et al.* (2002) used data from 39 X-ray emitting pulsars to find a best fit that describes the correlation between  $\log L_X$ - $\log \dot{E}$ . These 39 sources were divided in to subcategories as; *millisecond pulsar* ( $P \lesssim 10$  ms), *Crab-like* ( $\tau \sim 10^4$  years), *Vela-like* ( $\tau \sim 10^4$ - $10^5$  years), *Geminga-like* ( $\tau \gtrsim 10^5$  years, where substantial amount of the X-ray flux comes from the internal cooling) and finally *Old-pulsars* ( $\tau \gtrsim 10^6$  years). In Figure 4 we show a similar plot. In this plot we only include Crab, Vela and Geminga-like pulsars. We did not include millisecond pulsars because they are re-cycled and do not represent the naturally aging pulsars with the same  $\dot{E}$ . Also when converting countrates in to luminosities, Possenti *et al.* (2002) adopted a power-law spectrum with  $\Gamma = 2$  for all millisecond pulsars. Hence, the luminosities do not come from spectral analysis and rather from assumptions based on other pulsars. Also we excluded the three Old-pulsars because their fluxes were obtained by scaling their *ROSAT* countrates to that of PSR B1929+10.

This newly formed set of pulsars represent the evolution of pulsars on the  $\log L_X$ - $\log \dot{E}$  plane. Where older pulsars are on the bottom left (low  $\dot{E}$ ) and young Crab-like pulsars are on the top right (high  $\dot{E}$ ). Using only these three subclasses (26 sources) we performed a linear fit of the form  $\log L_X = a \log \dot{E} + b$  (see Figure 4). Due to exclusion of the stated pulsars our fit yields a line with a steeper slope ( $m \sim 1.5$ ). We also identified the line of maximum efficiency as the line for which every pulsar lies underneath. We then overlayed only three of the seven old pulsars, with well known spectra. We should note that, however, with their luminosities derived from the power-law fits, PSR B0943+10 (Zhang *et al.* 2005) and PSR B2224+65 (Zavlin & Pavlov 2004), have efficiencies exceeding the maximum efficiency.

From Figure 4 it is apparent that old pulsars have very high nonthermal X-ray efficiencies. This is contrary to what Possenti *et al.* (2002) has found and to what has been found when millisecond pulsars were excluded. The observed luminosities for younger pulsars also show large deviations, from this dependence. But in their case the deviation is symmetric around the trend line. The scatter that young pulsars exhibit could be due to uncertainties in pulsar distances (although they have been accounted for when calculating the errors), spread in the orientations of magnetic and rotational axes versus the line of sight. For example, seeing a certain fraction of the beam would result in lower inferred X-ray efficiency and vice versa.

Although there should be a thermal contribution to the overall luminosity, this effect will not change the nonthermal luminosity significantly. For instance, when we subtract the thermal luminosity, obtained for PSR B0628-28 (see § 3.2), from the total, the nonthermal luminosity only changes by a factor of 0.5. The resulting luminosity is still too big and gives a nonthermal X-ray efficiency 2-3 orders of magnitudes greater than the maximum efficiency.

The photon indices of these luminous old pulsars on the average is larger than those of their younger counterparts. The mean of the photon indices of the 26 pulsars is 1.85 as opposed to 2.51 for the old pulsars. The spectra of these old pulsars being steeper should result in lower luminosities in the 2-10 keV band. However, we observe an inverse effect where not only the spectra are steeper but also they have higher luminosities. Further X-ray observations of old radio pulsars should help us understand these puzzling features.

## REFERENCES

Becker, W., Weisskopf, M.C., Tenant, A.F., Jessner, A., Dyks, J., Harding, A.K., & Zhang, S.N., 2004, *ApJ*, 615, 908

Cordes, J.M., & Lazio, T.J.W., 2002, preprint (astro-ph/0207156)

Ögelman, H.B., & Tepedelenlioğlu, 2004, *Adv. Space Res.*, 33(4), 597

Possenti, A., Cerutti, R., Colpi, M., Mereghetti, S., 2002, *A&A*, 387, 993

Shibasaki, N., & Lamb, F.K., 1989, *ApJ*, 346, 808

Tsuruta, S., 1998, *Phys. Rep.*, 292, 1

Zavlin, V.E., & Pavlov, G.G., 2004, *ApJ*, 616, 452

Zhang, B., Sanwal, D., & Pavlov, G.G., 2005, preprint (astro-ph/0503423)

Table 1. Properties of PSR B0628-28 derived from radio observations

| Parameter   | Value                      |
|---|----------------------------|
| Frequency (Hz).....   | 0.80358811986              |
| Frequency derivative (Hz s <sup>-1</sup> ).....               | -4.59962×10 <sup>-15</sup> |
| Epoch (MJD).....  | 46603.0                    |
| Spin-down age (10 <sup>6</sup> yr).....                       | 2.77                       |
| Spin-down energy (10 <sup>32</sup> ergs s <sup>-1</sup> ).... | 1.5                        |
| Inferred Magnetic Field (10 <sup>12</sup> G)...               | 3.0                        |
| Dispersion Measure (pc cm <sup>-3</sup> ).....                | 34.5                       |
| Distance (kpc).....   | 1.45                       |

Note. — Distance is inferred from dispersion-measure (Cordes & Lazio 2002).

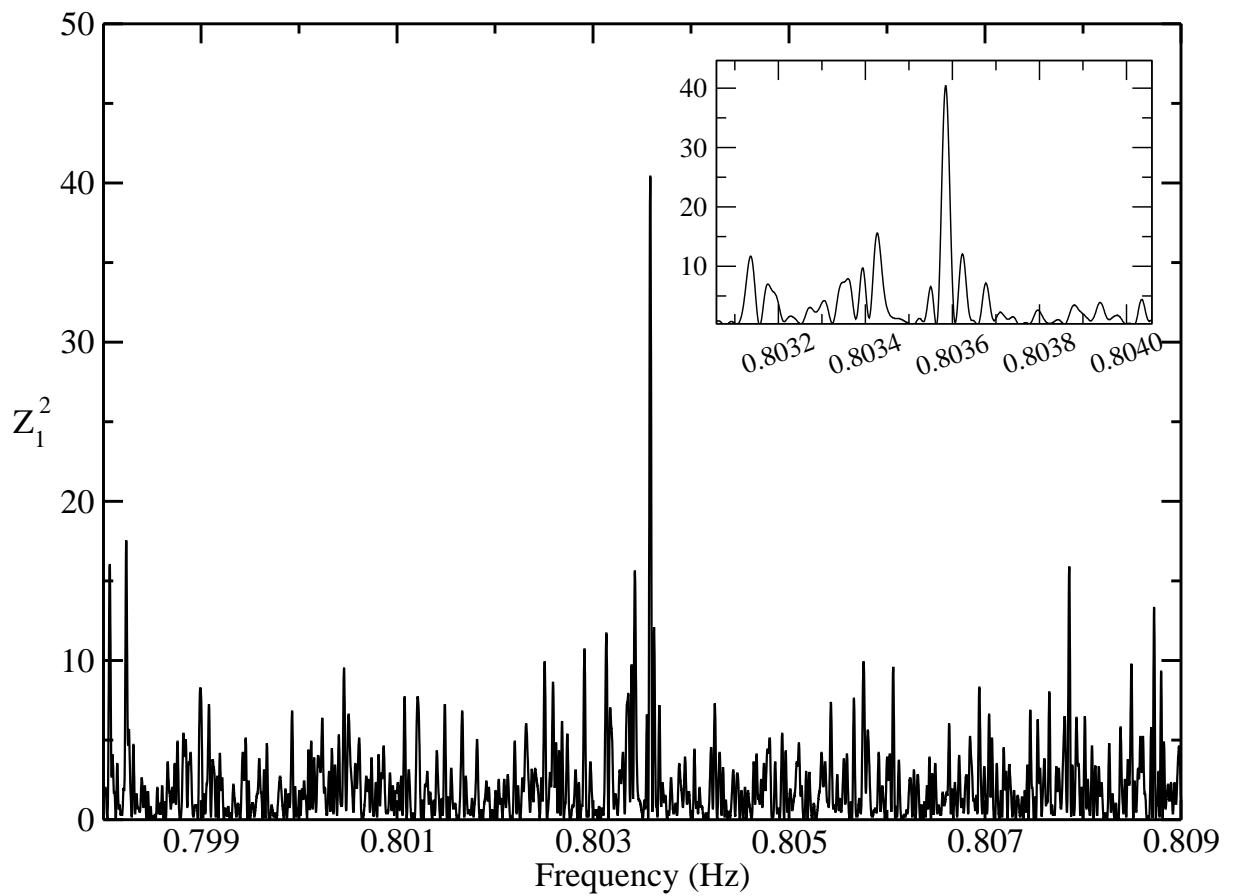


Fig. 1.— The power spectrum of the timing data around the expected frequency. The inset is the expanded view  $\pm 500 \mu\text{Hz}$  around the peak, which is located at  $f = 0.80358551 \text{ Hz}$ .

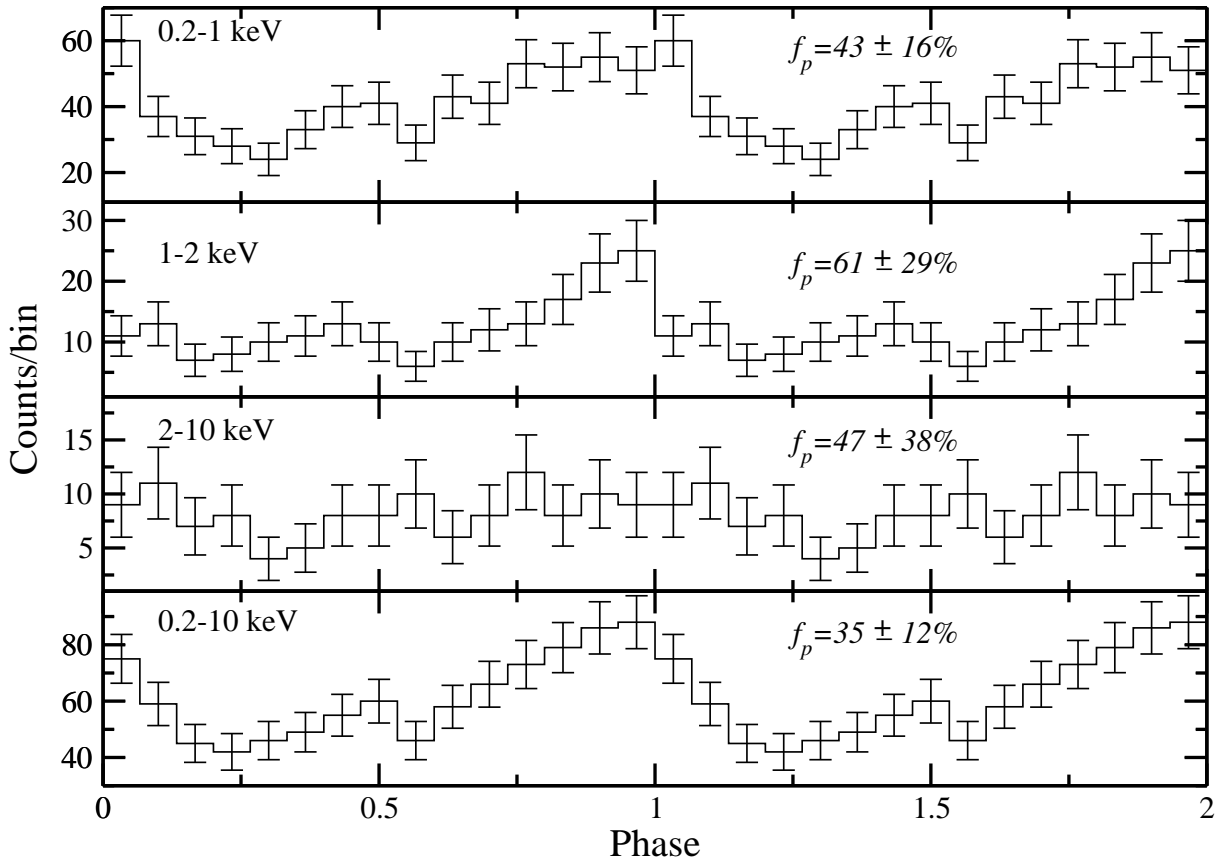


Fig. 2.— X-ray light curves of PSR B0628-28 extracted from the EPIC-pn data in four energy bands, with the values of the intrinsic pulsed fraction  $f_p$  and its  $1\sigma$  errors. Two phase cycles are shown for clarity. For the expression used for the pulse fraction see text.

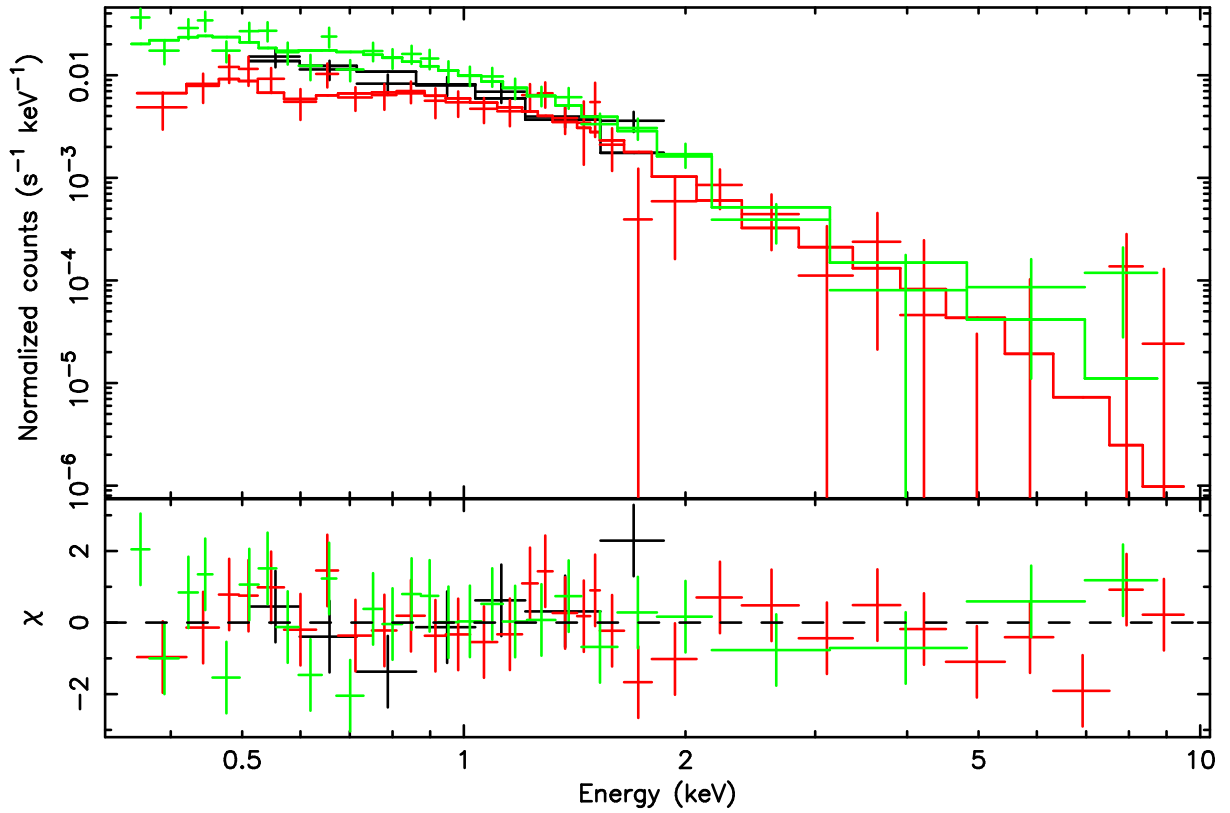


Fig. 3.— Energy spectrum of PSR B0628-28 as observed with pn (upper spectrum), MOS1/2 (lower spectrum) and ACIS-S (middle spectrum). The lines are the best fit power-law model. The lower panel is fit residuals.

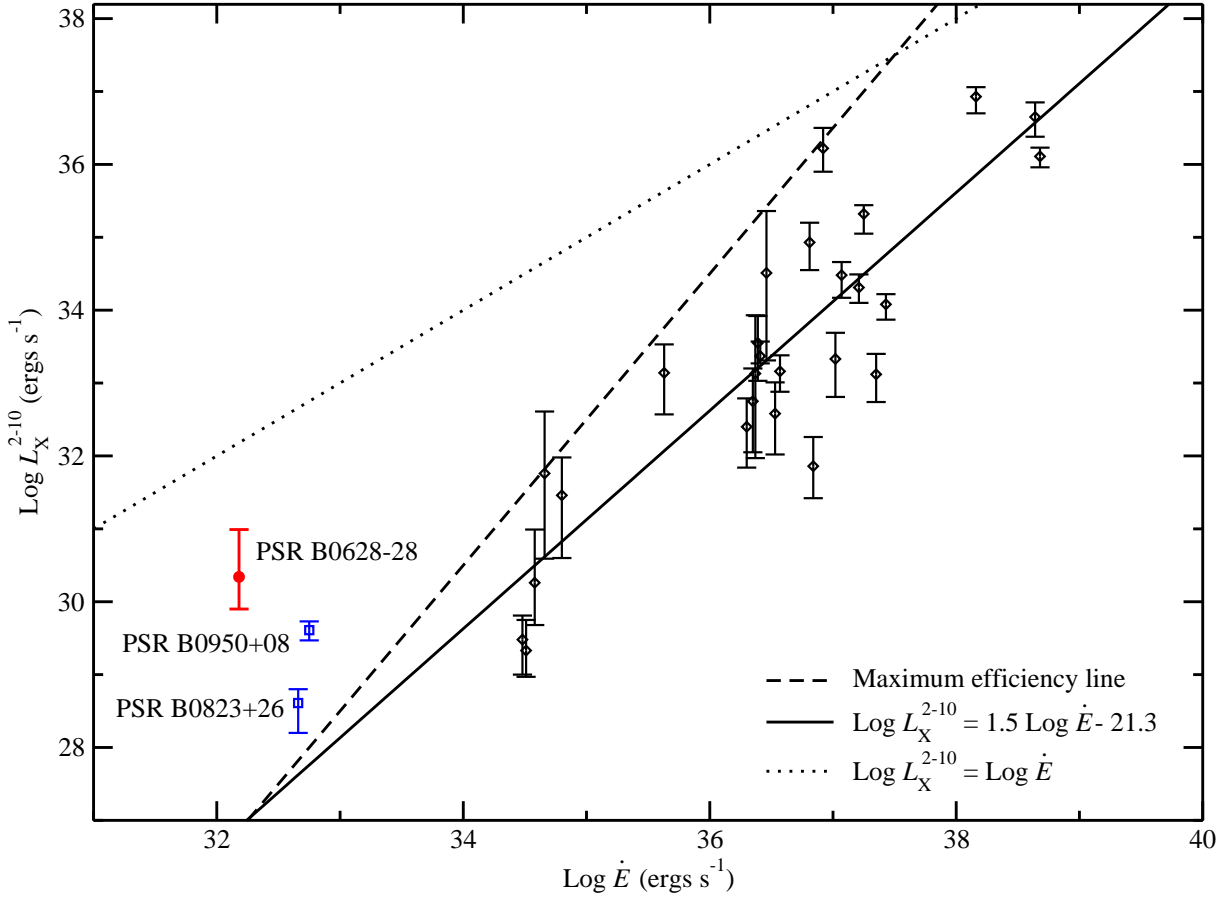


Fig. 4.— The X-ray luminosity in the band 2-10 keV versus the spin-down power for the 26 sources together with three old pulsars. The value for the X-ray luminosities of PSRs B0950+08 and B0823+26 are taken from Becker *et al.* (2004) and the rest are taken from Possenti *et al.* (2002). The solid line is the best fit to the set of 26 pulsars. Other two lines are labeled in the legend.